RESEARCH PAPER

Green synthesis of carbon dots using the flowers of *Osmanthus fragrans* (Thunb.) Lour. as precursors: application in Fe^{3+} and ascorbic acid determination and cell imaging

Min Wang[1] · Yuyan Wan[1] · Kailian Zhang[1] · Qifeng Fu[1] · Lujun Wang[1] · Jing Zeng[1] · Zhining Xia[2] · Die Gao[1]

Abstract

In this work, dried flowers of *Osmanthus fragrans* Lour. were applied as green precursors to synthesize carbon dots (CDs) by a green hydrothermal method for the first time. The CDs showed strong blue fluorescence at 410 nm under 340-nm excitation with a quantum yield of approximately 18.53%. Furthermore, the CDs were applied for the sensitive detection of Fe^{3+}. The linear response of Fe^{3+} ranged from 10 nM to 50 μM with a limit of detection as low as 5 nM. In addition, other ions were used as competitive substances to explore the selectivity of CDs for Fe^{3+}. The fluorescence quenching effect of Fe^{3+} was much stronger, which demonstrated that the CDs had high selectivity for Fe^{3+} and they can be employed for the selective detection of Fe^{3+}. The potential fluorescence quenching mechanism between CDs and Fe^{3+} was identified as the inner filter effect. The CDs were then used as a fluorescent sensor for the detection of Fe^{3+} in water samples and human serum; the recovery range was 93.76–113.80% (relative standard deviation less than 0.79%). These results indicate that the CDs can be applied for the sensitive and selective detection of Fe^{3+} in real samples. Moreover, on the basis of the redox reaction between Fe^{3+} and ascorbic acid (AA), the CD–Fe^{3+} system can be used as a fluorescent "off–on" sensor for the detection of AA with a limit of detection of 5 μM. What is more, because of their low toxicity and biocompatibility, the CDs can also be used for cell imaging and acted as a fluorescent probe for fluorescence imaging of Fe^{3+} and AA in living cells. These results demonstrate that the CDs have great potential for application in the fields of sensing, bioimaging, and even disease diagnosis.

Keywords Carbon dots · Flowers of *Osmanthus fragrans* Lour. · Fe^{3+} · Inner filter effect · Fluorescent "off–on" sensor · Ascorbic acid

Introduction

Carbon dots (CDs), a new type of carbon nanomaterial with a diameter less than 10 nm, are regarded as a rising star among fluorescent materials owing to their outstanding fluorescence properties [1]. Because of outstanding advantages such as simple preparation, good fluorescence properties, good water solubility, and low toxicity [2–4], they have attracted tremendous interest in the fields of sensing [5], bioimaging [6], and drug delivery [7]. Because of their multimodal applications, various synthetic methods, such as the solvothermal method (including a hydrothermal method) [8, 9], the microwave method [10], and chemical oxidation [11], have been developed for the preparation of CDs. Among these methods, the solvothermal method has been applied most commonly as it is convenient and efficient. However, to obtain CDs with high quantum yield (QY), this commonly used method suffers from several limitations, such as the selection of precursors and the toxicity of solvents. Usually, the common used precursors in solventhermal method are citric acid coupled with urea [12], ethanediamine [13], tris (hydroxymethyl) methyl

✉ Zhining Xia
tcm_anal_cqu@163.com

✉ Die Gao
gaodie_1203@126.com

1   School of Pharmacy, Southwest Medical University, Luzhou 646000, Sichuan, China

2   School of Pharmaceutical Sciences, Chongqing University, Chongqing 401331, China

aminomethane [14] and etc. Moreover, some reactions even need to use toxic solvents such as toluene [15] or dimethyl fumarate [16] to obtain CDs with high QY. The use of these chemicals and toxic solvents does not meet the standard of green chemistry and is harmful to humans. Therefore, there is a need to explore a green synthetic approach for the preparation of CDs by use of green precursors and nontoxic solvents.

Lately, various natural raw materials, such as milk [17], pseudostem of the banana plant [18], onion waste [19], *Lantana camara* berries [20], and tulsi leaves [21], have been used as green precursors for the preparation of CDs by a green hydrothermal method. Because of the presence of multiple components, the CDs prepared with these natural raw materials have tunable surface functional groups. These groups can improve the photoluminescence properties of CDs, resulting in increased sensitivity and selectivity of CDs for target molecules. Xu et al. [22] prepared CDs by using ginkgo leaf as a green precursor. The CDs were used for ultrasensitive, highly selective detection of Pb^{2+} with a limit of detection (LOD) of 55 pM. In addition, these CDs prepared with green precursors and with water as a solvent have good water solubility and biocompatibility and can be applied in the bioimaging field [23]. Li et al. [24] prepared CDs by using *Brassica compestris* L. var. *purpurea* Bailey as a precursor and water as a solvent: The CDs had low cytotoxicity toward HepG2 cells and labeled them successfully. From these points, preparation of CDs with good physicochemical and photoluminescence properties by use of green precursors and a green synthetic method is very desirable.

The flowers of *Osmanthus fragrans* Lour., also named "Guihua" in China, are especially famous as their essential oil can be widely used in aromatherapy and to produce perfumes [25, 26]. They also exhibit many pharmacological activities, such as antioxidant and antitumor activities [25, 27]. The flowers of *O. fragrans* are rich in flavonoids, phenylethanoid glycosides, and phenolic acids [28]. The diversity of the constituents makes the flowers a potential natural raw material for the preparation of CDs. Moreover, flavonoids in the flowers can easily interact with metal ions such as Fe^{3+} and Pb^{2+} [29, 30]. Hence, CDs prepared with flowers of *O. fragrans* as green precursors may be used for the detection of metal ions. In addition, as the planting of *O. fragrans* in China is widespread, many flowers of *O. fragrans* are discarded and not fully utilized. Therefore, use of the flowers of *O. fragrans* as precursors is also an effective method to maximize the utilization of natural resources.

In present study, flowers of *O. fragrans* were used as green precursors for the preparation of new CDs by a simple hydrothermal method for the first time. By use of this method, high-quality CDs with a QY of 18.53% can be produced on a large scale without the assistance of any chemical reagent. Optical and chemical properties of the CDs were characterized by UV–visible (UV–vis) absorption spectroscopy, fluorescence

spectroscopy, X-ray diffraction (XRD), Fourier transform IR (FT-IR) spectroscopy, transmission electron microscopy (TEM), X-ray photoelectron spectroscopy (XPS), and energy-dispersive X-ray spectroscopy (EDS). Because CDs prepared with the flowers of *O. fragrans* as precursors have potential in metal ion detection, the CDs were applied for the fluorescent detection of Fe^{3+}. They showed high sensitivity and selectivity toward Fe^{3+} with a linear range of 10 nM to 50 μM. The LOD of Fe^{3+} detection was 5 nM, which was lower than for previously reported CDs (prepared with green precursors) [26, 31]. Moreover, the CD–Fe^{3+} quenching mechanism was studied by UV–vis detection and fluorescence lifetime determination. The mechanism was identified as the inner filter effect (IFE). Furthermore, the CDs were further applied to the detection of Fe^{3+} in real water samples and human serum with a recovery range of 93.8–113.8%, which confirms the good analytical performance of this CD-based sensor. The fluorescence of CDs quenched by Fe^{3+} can be partly recovered by addition of ascorbic acid (AA), and this change can be used for further detection of AA by an "off–on" sensor. Finally, to explore toxicity and biocompatibility, 3-(4,5-dimethylthiazol-2-yl)-2,5-diphenyltetrazolium bromide (MTT) measurement and cell imaging were conducted on a human lung cancer (A549) cell line. The results demonstrate that the CDs exhibited low toxicity and good biocompatibility with regard to A549 cells, and Fe^{3+} (AA) can also be qualitatively analyzed by monitoring of the changes in cell fluorescence. In general, the CDs have great potential for application in detection of Fe^{3+} and AA and can be used as a fluorescent probe for cell imaging.

Experimental

Chemicals and reagents

The flowers of *O. fragrans* were picked from Southwest Medical University (Luzhou, China) and dried at room temperature. Quinine sulfate (purity greater than 99%) was bought from Acros Co. (https://www.acros.com). AA and reagents related to ions were purchased from Kelong Chemical Co. (http://www.cdkelong.com/cn). A549 cells were obtained from the Cell Center of the Chinese Academy of Medicinal Sciences (http://cellbank.bioon.com.cn). Phosphate-buffered saline (PBS), penicillin–streptomycin, and MTT were obtained from Beijing Dingguo Biotechnology Co. (http://www.dingguo.com). Dulbecco's modified Eagle's medium (DMEM), fetal bovine serum (FBS) and trypsin were obtained from Gibco (https://www.fishersci.com). Ultrapure water was used in all aqueous solutions in the whole experiment process.

Instruments

The UV–vis absorption spectra of CDs were obtained with a UV-2600 spectrometer (Shimadzu, https://www.shimadzu.com). The fluorescence spectra of CDs were obtained with an LS-55 fluorescence spectrometer (PerkinElmer, http://www.perkinelmer.com.cn). A JEM 2100 transmission electron microscope (JEOL, https://www.jeol.co.jp) was used to acquire the TEM image. XRD measurements were performed with an Ultima IV X-ray diffractometer (Pabakytucal X′Pert Powder, http://www.spectris.com). FT-IR spectra were obtained with an IRAffinity-1S FT-IR spectrophotometer (Shimadzu, https://www.shimadzu.com). XPS spectra were obtained with an ESCALAB 250Xi X-ray photoelectron spectrometer (Thermo Electron, https://www.thermofisher.com). EDS was conducted with an EX-250 energy-dispersive X-ray analyzer (Horiba, https://www.horiba.com). Fluorescence images of cells were recorded with an IX-73 inverted fluorescence microscope (Olympus, http://cn.olympus.com). The fluorescence lifetimes were obtained with an FLS980 lifetime and steady-state spectrometer (Edinburgh Instruments, https://www.edinst.com).

Preparation of CDs

A facile one-step hydrothermal method was used to synthesize CDs by use of flowers of *O. fragrans* as green precursors. Firstly, 35 mL of ultrapure water was added to 2 g of dried *O. fragrans* flowers and the mixture was ultrasonicated for 30 min until the water changed from white to brown. Then the mixture was transferred to a 50-mL Teflon-lined stainless-steel autoclave and heated at 240 °C for 5 h. After cooling to room temperature, the upper yellow-brown solution was centrifuged at 10,000 rpm for 10 min to remove most of the impurities, and was then filtered through a 0.22-μm membrane filter. The solution was dialyzed through a dialysis membrane (3000-Da tubing) for 48 h, and then the final CDs were obtained.

Fluorescence assay of Fe^{3+} and AA

All the Fe^{3+} detection experiments were performed under the same conditions at pH 6 in 10 mM PBS and the fluorescence intensity was recorded at an excitation wavelength of 340 nm. Other ions (including Fe^{2+}, Zn^{2+}, Ba^{2+}, Mn^{2+}, Al^{3+}, Co^{2+}, Mo^{4+}, K^+, Cd^{2+}, Pb^{2+}, Cu^{2+}, Ni^{2+}, Mg^{2+}, Ca^{2+}, HCO_3^-, HPO_4^-, NO_2^-, and SO_4^{2-}) were used to determine the selectivity of the CDs for Fe^{3+} under the same experimental conditions. To evaluate the sensitivity of the CDs for Fe^{3+}, different concentrations of Fe^{3+} (300 μL) were added to aqueous solutions of CDs (6 μg mL^{-1}, 2.7 mL) and the mixture solutions were measured by the fluorescence spectrometer.

For detection of AA, 300 μL of different concentrations of AA was mixed with 2.7 mL of the CD–Fe^{3+} mixture solution (the concentration of Fe^{3+} was 0.5 mM and the concentration of the CDs was 6 μg mL^{-1}). The fluorescence spectra were obtained at an excitation wavelength of 340 nm.

Determination of Fe^{3+} in real samples

The pretreatment of water samples and the human serum sample is described in the electronic supplementary material. To calculate the recoveries of Fe^{3+} in the real samples, different concentrations of Fe^{3+} standard solutions were added the CD solution directly by the standard addition method. The fluorescence intensities were measured with the fluorescence spectrometer at excitation and emission wavelengths of 340 and 410 nm, respectively. Moreover, the experiment was performed three times under the same experimental conditions to obtain the relative standard deviation.

Application of CDs in living cells

MTT measurement

To explore the biocompatibility and cytotoxicity of CDs, MTT measurement was done on A549 cells. Cells were seeded in 96-well plates and incubated for 24 h in a CO_2 incubator. Then different concentrations of CDs were added to the wells and incubation was performed for another 24 h. Next, 10 μL of MTT (5.0 mg mL^{-1}) was added to each well and the resulting mixture was incubated at 37 ° C for 4 h. The solutions in all wells were then removed and 150 μL of dimethyl sulfoxide was added to each well to dissolve the formazan complex. The plate was shaken for 10 min before testing. Finally, the absorbance was detected at 570 nm by use of a Synergy H1 microplate reader (Biotek, https://www.biotek.com).

Cell imaging

The A549 cells were cultured in DMEM medium (containing 10% FBS) in six-well plates and incubated for 24 h at 37 °C until confluency. The cells were then treated with CDs at 1 mg mL^{-1} (by addition of 10 μL) for 3 h. Then DMEM was removed and A549 cells were washed with PBS (pH 7.4) three times and then kept in PBS. The CD-labeled cells were then treated with Fe^{3+} (0.4 mM) and incubated for 30 min for further fluorescence imaging. Finally, AA solution (0.4 mM) was added to the cells (with CDs and Fe^{3+}) and the resulting mixture was incubated for 30 min for fluorescence imaging. All the fluorescence images were collected at an excitation wavelength of 340 nm. The preparation process and applications of CDs are stated in Fig. 1.
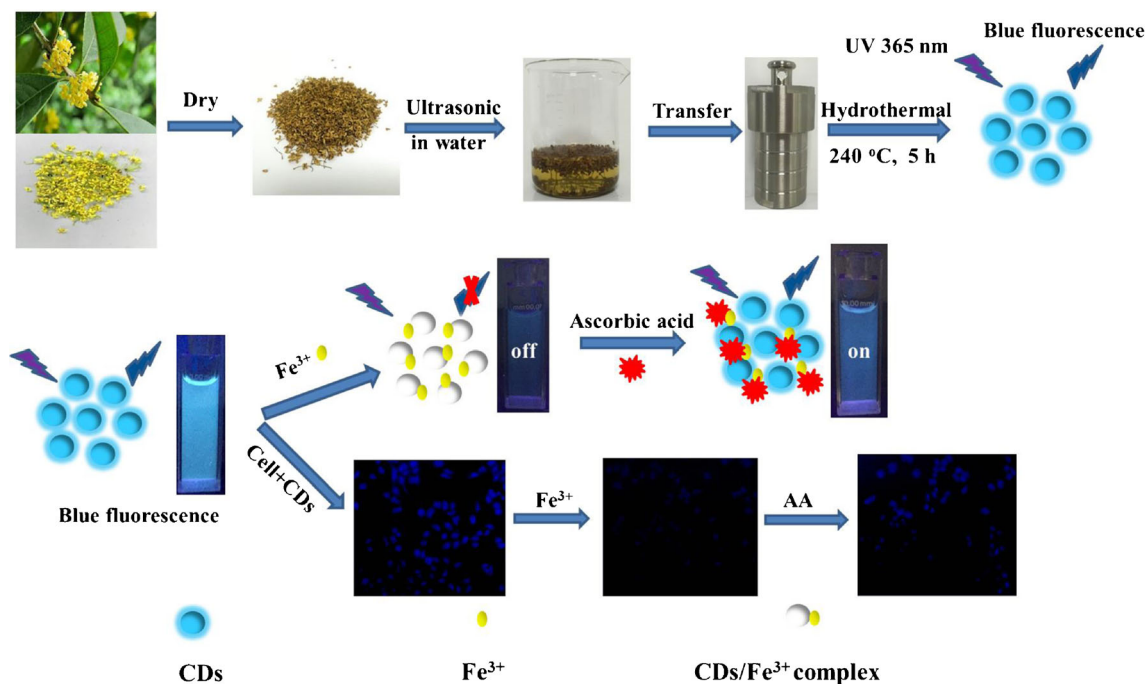
Fig. 1 The synthesis and application of carbon dots (CDs). AA ascorbic acid

Results and discussion

### Synthesis and characterization of CDs

Compared with traditional methods, the hydrothermal method is green and facile. Moreover, it is reported that the flowers of *O. fragrans* contain a large amount of flavonoids and glycosides, which are nontoxic and hydrophilic and so the CDs prepared with these constituents can easily and quickly disperse in water [32, 33]. Therefore, in the present work, CDs were synthesized via a one-step hydrothermal method by use of flowers of *O. fragrans* as green precursors and water as a solvent. To obtain CDs with high QY, three factors (the amount of the flowers of *O. fragrans*, the reaction temperature, and the reaction time) influencing the QY were optimized. As shown in Table S1, the highest QY obtained was 18.53% by use of 2 g of flowers of *O. fragrans* as raw materials, 240 °C as the reaction temperature and 5 h as the reaction time

The morphology of the CDs was revealed by TEM. As shown in Fig. 2a, the TEM image of the CDs revealed that the average diameter of the CDs was about 2.23 nm, and it can be clearly seen that the size distribution was relatively uniform and the size differentiation was relatively small (Fig. 2b). In addition, the crystalline nature of the CDs was confirmed by XRD analysis. The XRD pattern of the CDs in Fig. 2c shows a broad diffraction peak centered at $2\theta = 26.7°$ attributed to the (002) lattice spacing of the graphitic carbon, and this indicated that the CDs contained graphite-like structures [34, 35].

The composition and functional groups of the CDs were identified by FT-IR spectroscopy. In Fig. 2d the absorption bands at 3418 and 3239 cm^{-1} correspond to O–H and N–H stretching vibrations. These two functional groups can increase the hydrophilicity and stability of the CDs [36, 37]. Moreover, the small peak at 2953 cm^{-1} is identified as the stretching vibration of C–H bonds. And the peaks at 1663 cm^{-1}, 1584 cm^{-1} and 1405 cm^{-1} were attributed to the C=O, C=C and CH$_2$ stretching bending vibrations, respectively [38]. In addition, the band at 1069 cm^{-1} is ascribed to the stretching vibration of C–O. These results indicate that –OH, –NH$_2$, and –COOH may exist on the surface of CDs. To further explore the elemental composition of the CDs, the EDS spectrum (Fig. S1) was obtained, and the results show that the CDs were composed of carbon (64.57%), nitrogen (3.1%), and oxygen (31.33%).

Furthermore, XPS was used for surface elemental analysis of the CDs. As depicted in Fig. 3a, the three strong typical peaks in the XPS spectrum of the CDs at 284.82, 399.84, and 531.89 eV belong to C 1s, N 1s, and O 1s. This indicates that the surface of the CDs was mainly composed of carbon, oxygen, and nitrogen [39, 40]. In detail, there were four main peaks in the high-resolution XPS spectrum of C 1s centered at 284.51, 285.69, 286.31, and 288.05 eV, which were assigned to C=C, C–N, C–OH, and C=O, respectively (Fig. 3b) [41]. However, the N 1s expanded spectrum (Fig. 3c) can be deconvoluted into three distinct carbon states at 387.90, 399.47, and 400.99 eV, which correspond to C–N–C, N–H, and C$_3$–N, respectively [42]. In addition, as shown in Fig. 3d, two peaks appeared in the O 1s expanded spectrum, at 530.99 and 532.28 eV, which are associated with C=O (sp^2) and C–O
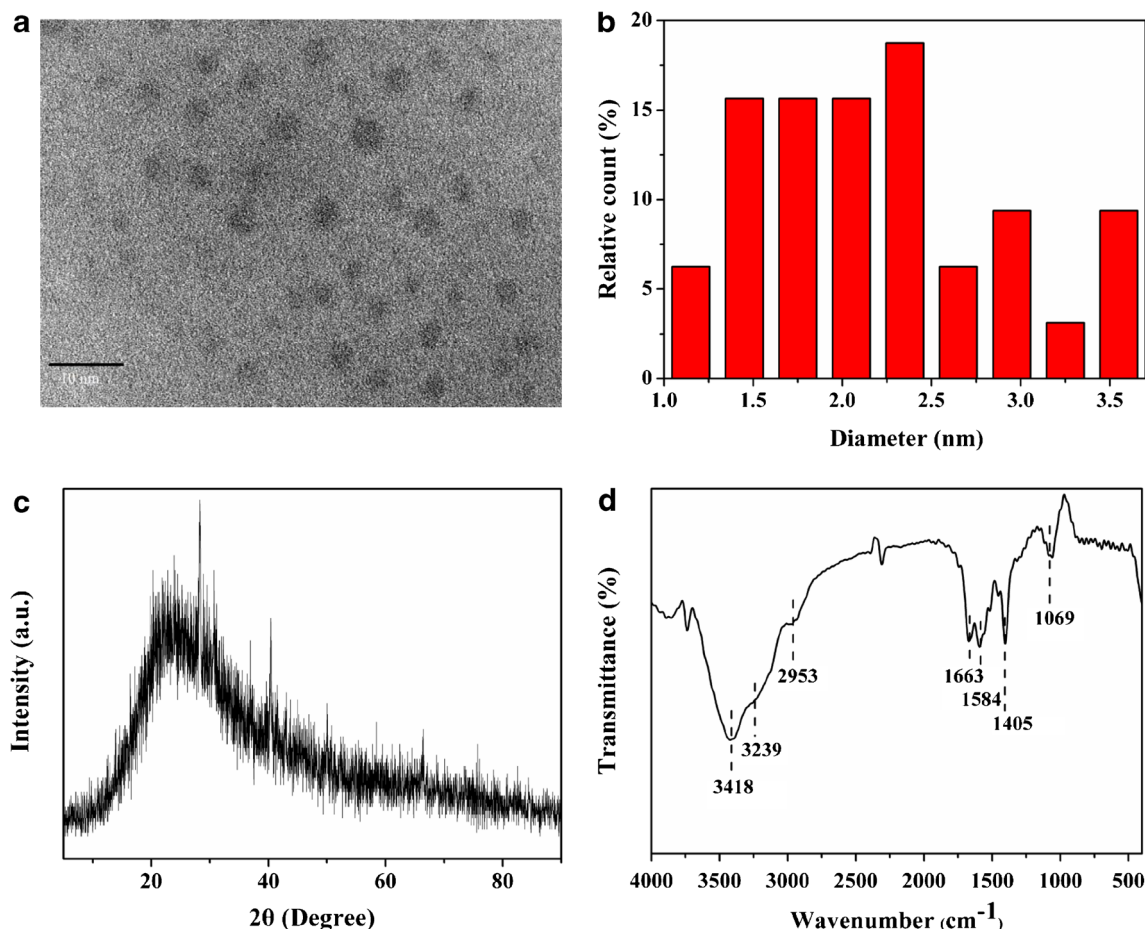
Fig. 2 **a** Transmission electron microscopy image of carbon dots (CDs). **b** Particle size distribution of CDs. **c** X-ray diffraction pattern of CDs. **d** Fourier transform IR spectrum of CDs

(sp^3), respectively [43]. These results indicate that the CDs contained C=C, $–NH_2$, and –COOH groups, which was in accordance with the results of FT-IR spectroscopy.

Optical properties of CDs

The absorption and fluorescence properties of the CDs were studied by UV–vis absorption spectroscopy and fluorescence spectroscopy. Figure 4a shows the UV absorption spectrum of the CDs from 200 to 600 nm. It can be obviously seen that there was an obvious absorption peak at around 280 nm, this peak was corresponded to the $n–\pi^*$ electronic transition of C=O banded on CDs [44]. Figure 4b reveals that the CDs exhibited strong blue fluorescence at 410 nm when excited at 340 nm. Moreover, from the inset in Fig. 4b, it can be easily seen that the CD solution was almost colorless in daylight and emitted bright blue fluorescence under excitation at 365 nm. Figure 4c shows the different emission wavelengths of the CDs obtained with different excitation wavelengths (ranging from 300 to 420 nm with a 10-nm increment). Furthermore, the corresponding normalized spectra are displayed in Fig. 4d. As the excitation wavelength increased, the emission wavelength

redshifted. This phenomenon resulted from the different surface states of CDs produced by different functional groups on the surface of the CDs and different sizes of the CDs [45].

Fluorescence response of CDs to Fe^{3+}

Optimization of the experimental conditions

The effects of pH, ionic strength, and solvent on the fluorescence intensities of the CDs were explored first. Respective results are given in Fig. S2. The optimized conditions for maintaining the CDs' performance were as follows: (a) pH 6 was the optimum pH; (b) the optimum ionic strength was 0 M NaCl (almost no effect on the detection); and (c) the solvent for CD dispersion was water. Further, the stability of the CDs in water was studied for 120 min. Figure S2d shows that the fluorescence intensity was almost invariable for 120 min, indicating that the CDs had good stability.

Furthermore, to exclude some possible interferences and screen the best detection conditions for Fe^{3+}, the following parameters for Fe^{3+} detection (the Fe^{3+} concentration used was 50 μM) were optimized: (a) the concentration of CDs,
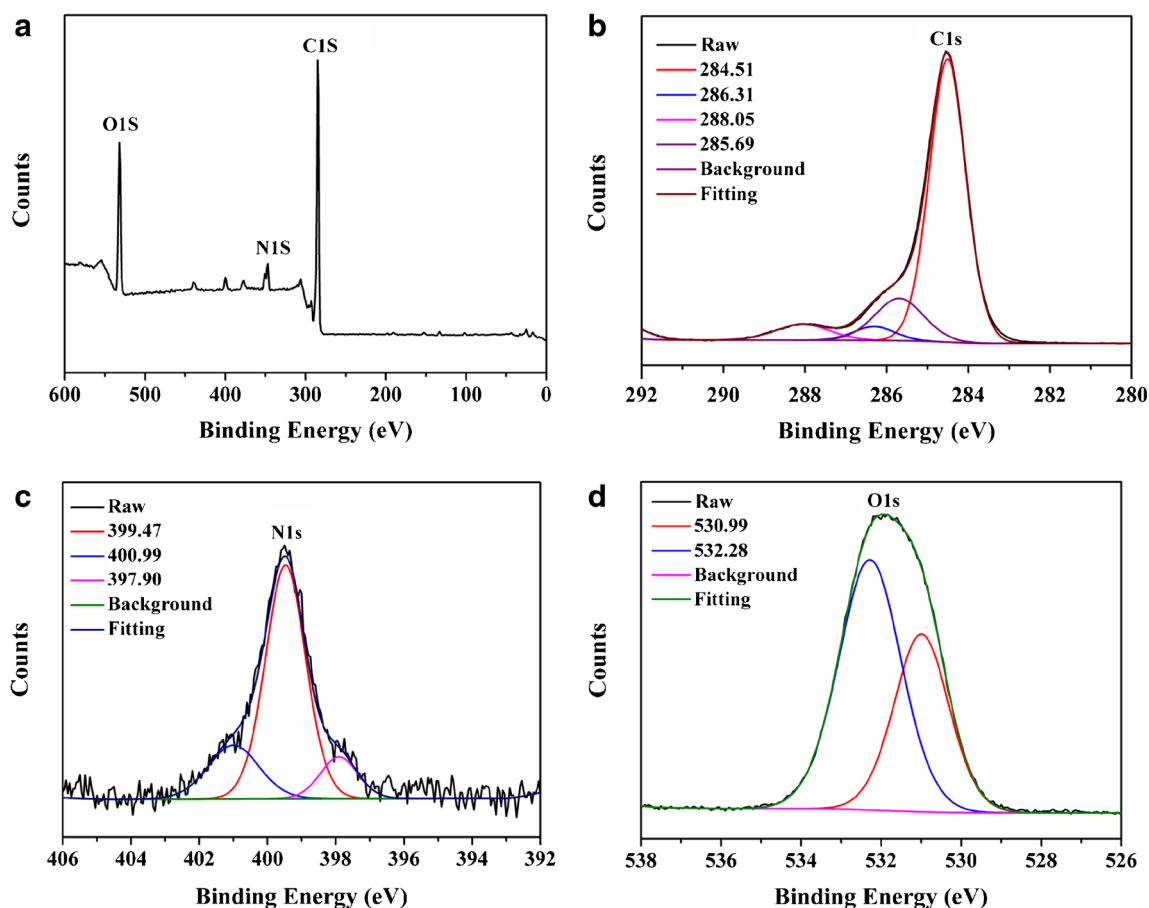
Fig. 3 **a** X-ray photoelectron spectroscopy spectra of carbon dots (CDs). **b** C 1*s* spectrum of CDs. **c** N 1*s* spectrum of CDs. **d** O 1*s* spectrum of CDs

(b) the pH, (c) the concentration of NaCl, and (d) the type of solvent. Respective plots are given in Fig. S3. The optimized conditions for Fe^{3+} detection were as follows: (a) CD concentration of 6 $\mu g \cdot mL^{-1}$, (b) pH 6, (c) 0 M NaCl, and (d) water solvent. These results demonstrated the best conditions (pH, ionic strength, and solvent) for Fe^{3+} detection were in accordance with the best conditions for maintaining the CDs' performance.

Selectivity and sensitivity for the detection of Fe^{3+}

The sensing performance of the CDs was assessed by selectivity experiments with various ions. The fluorescence intensities were investigated by our adding different ions (Fe^{2+}, Zn^{2+}, Ba^{2+}, Mn^{2+}, Al^{3+}, Co^{2+}, Mo^{4+}, K^+, Cd^{2+}, Pb^{2+}, Cu^{2+}, Ni^{2+}, Mg^{2+}, Ca^{2+}, HCO_3^-, HPO_4^-, NO_2^-, SO_4^{2-}, and Fe^{3+}) in 0.3 mM concentration to CD solutions (6 $\mu g \cdot mL^{-1}$). From Fig. 5a, it is clearly seen that Fe^{3+} showed the strongest fluorescence quenching effect on CDs, whereas there were no remarkable fluorescence changes for the other ions. Moreover, to further determine the selectivity of CDs for Fe^{3+}, 0.3 mM Fe^{3+} was added to a solution of CDs containing other ions in 0.3 mM concentration. The results revealed that the CDs had high selectivity for the detection of Fe^{3+} and can be used as a

good fluorescent sensor for Fe^{3+} detection. This good selectivity of the CDs for Fe^{3+} was mainly attributed to photoelectron transfer caused by the strong affinity interaction between Fe^{3+} and the –COOH and –OH groups on the surface of the CDs. Fe^{3+} had faster chelating kinetics in comparison with the other ions [46, 47]. All these reasons can cause the electrons of the CDs in the excited state to be transferred to the unfilled orbital of Fe^{3+} and resulted in nonradiative electron–hole recombination, causing fluorescence quenching [39].

From Fig. 1, it is very apparent that the fluorescence of the CDs almost disappears under 365-nm light after addition of 0.3 mM Fe^{3+} to the CD solution. To further study the sensitivity of the CDs for Fe^{3+}, the fluorescence of the CDs was investigated by our adding different concentrations of Fe^{3+} (0–500 μM) under the optimum conditions. Figure 5b shows that as the concentration of Fe^{3+} increased, the fluorescence intensity of the CDs gradually decreased. The relationship between F_0/F and the concentration of Fe^{3+} is shown in Fig. 5c, where a good linear relationship was obtained in the range from 10 nM to 50 μM with a correlation coefficient (R^2) of 0.9992. The linear equation was $F_0/F = 0.0234C + 1.0412$, where C is the concentration of Fe^{3+}. On the basis of three times the standard deviation of 11 measurements of the blank signal of the CD solution, the LOD was found to be 5 nM,
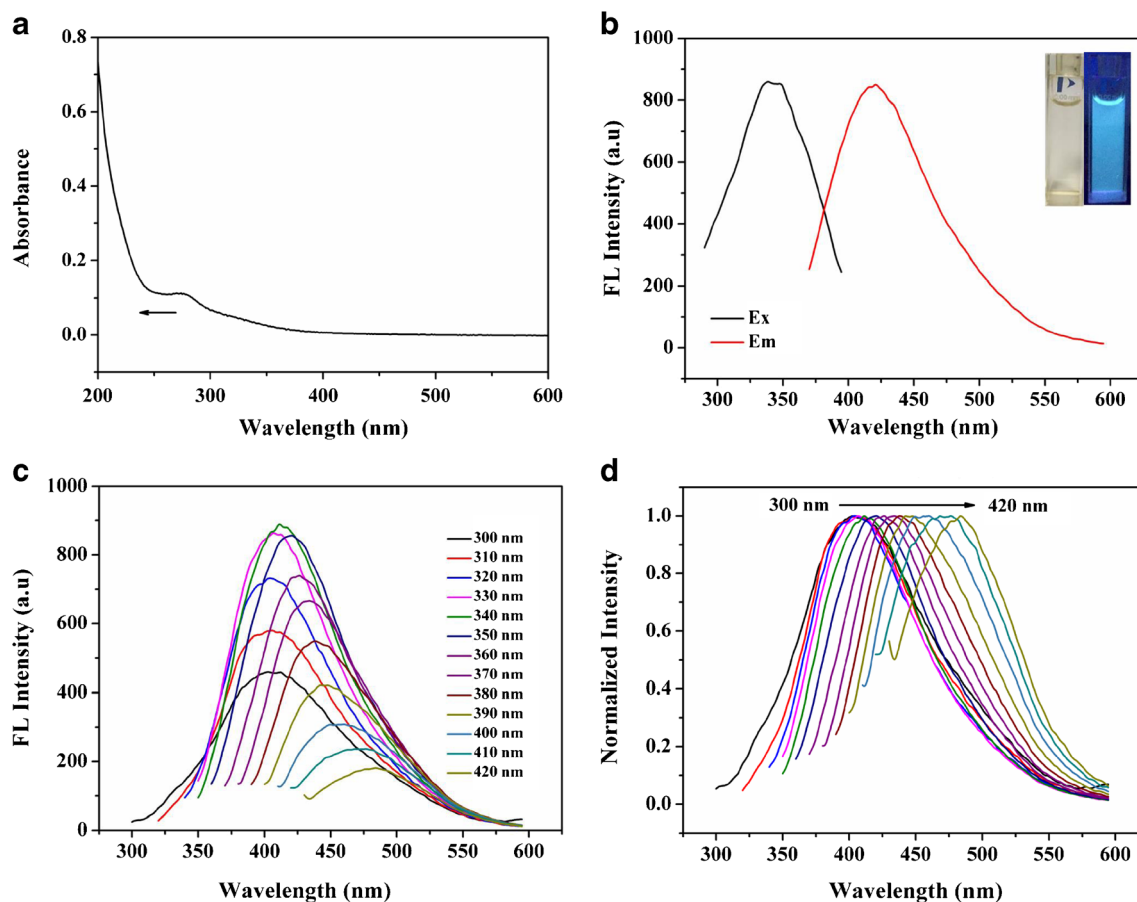
Fig. 4 **a** UV–vis absorption spectrum of carbon dots (CDs). **b** Fluorescence excitation spectrum and emission spectrum of CDs. The insets display images of the CDs in daylight and under 365-nm light. **c** Excitation-wavelength-dependent emission spectra from 300 to 420 nm. **d** Normalized emission spectra of CDs with different excitation wavelengths. FL fluorescence

which is lower than previously reported in the literature (listed in Table S2). These results indicate that the CDs showed high sensitivity for Fe^{3+}, and the wide linear range and low LOD confirmed that the CDs can be used as a good fluorescent sensor.

Detection of Fe^{3+} in real samples

As Fe^{3+} is one of the most essential trace elements in the human body and water samples, its detection in real water samples and human serum samples is a good way to verify the applicability of the CDs. In the present work, tap water, two different river water samples (river water 1 representing Tuo River water and river water 2 representing Min River water), and human serum were chosen as the real samples to check the realistic application and the feasibility of the CDs. Different concentrations of Fe^{3+} (5, 10, and 50 μM) were added to the processed samples; the related recoveries are shown in Table 1. The recoveries of these samples ranged from 93.76% to 113.80% and the relative standard deviations were less than 1%. From these results, it can be summarized that the CDs had good performance in real samples and they

can be used to effectively detect Fe^{3+} in water and biological samples.

Quenching mechanism study of the CD–Fe^{3+} system

To investigate the quenching mechanism between CDs and Fe^{3+}, the UV–vis absorption spectra of Fe^{3+} and the fluorescence spectra of the CDs were studied. Figure 6a shows that there was obvious overlap between the excitation spectrum of the CDs and the absorption spectrum of Fe^{3+}. Because of this overlap, the enhancement of absorbance of Fe^{3+} can be successfully converted into fluorescence quenching of CDs [48]. As the IFE usually occurs when the excitation spectrum or emission spectrum of the donor has obvious overlap with the absorption spectrum of the acceptor, Fe^{3+} can quench the fluorescence of the CDs probably via the IFE [49]. The fluorescence decay spectra of the CDs with and without Fe^{3+} were investigated to further verify the mechanism. As shown in Fig. 6b, the fluorescence decay time of the CDs in the absence and presence of Fe^{3+} was analyzed by double-exponential fitting. Two decay lifetimes of
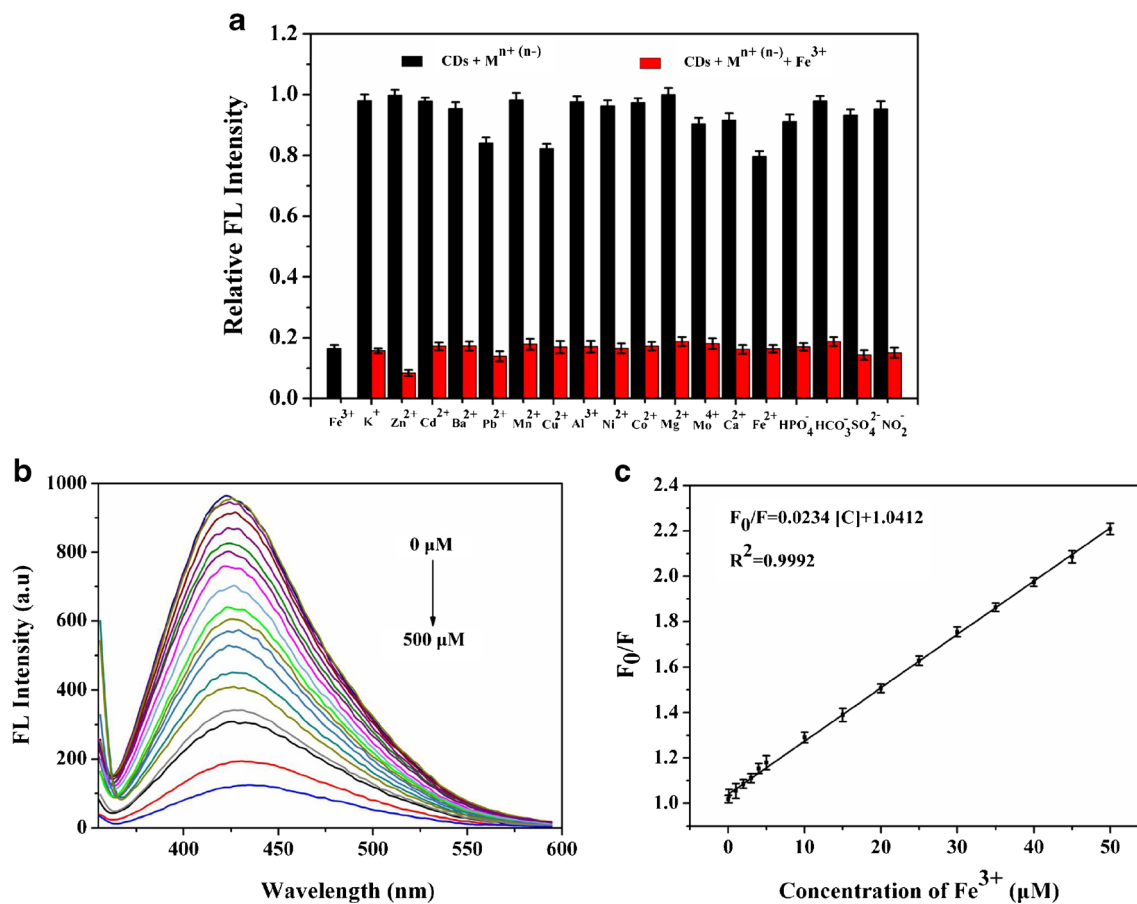
Fig. 5 a Selectivity of carbon dots (CDs) for Fe^{3+} over other ions. b Fluorescence spectra of CDs in the presence of different concentrations of Fe^{3+} (0–500 μM). c F_0/F versus Fe^{3+}concentration in the range from 10 nM to 50 μM, where F_0 and F are the fluorescence areas of the CDs in the absence and presence of Fe^{3+}. FL fluorescence

2.06625 and 7.56736 ns (χ^2 = 0.997) were obtained, whereas the lifetimes changed to 1.78886 and 7.48038 ns (χ^2 = 0.991) after addition of Fe^{3+} to the CD solution. The fluorescence lifetimes changed little after the addition of Fe^{3+} on fitting of the data, which indicated that static quenching existed and further confirms the existence of the IFE between the CDs and Fe^{3+} [48, 50, 51].

Fluorescence off–on detection of AA

Because of its strong oxidization, Fe^{3+} has an effect on substances with strong reducibility. Because AA is highly reductive, the redox reaction between Fe^{3+} and AA will lead to the oxidation of the enediol group in AA along with the reduction of Fe^{3+} to Fe^{2+} (shown in Eq. S1) [52, 53]. Therefore, the weak fluorescence in the CD–Fe^{3+} system may be partially recovered as some Fe^{3+} ions are converted into Fe^{2+} ions (shown in Fig. 7a). Therefore, the CD–Fe^{3+} system can be applied to detect AA by turning fluorescence off–on.

To optimize the detection conditions for AA, the effect of the response time was investigated. As shown in Fig. 7b, the fluorescence intensity immediately reduced after addition of 0.5 mM Fe^{3+} and then remained stable.

Table 1 Determination of Fe^{3+} in real samples with the proposed method ($n = 3$)

Sample	Added (μM)	Found (μM)	Recovery (%)	RSD (%)
Tap water	5	5.53 ± 0.041	110.60 ± 0.82	0.74
	10	10.76 ± 0.074	107.60 ± 0.74	0.69
	50	46.88 ± 0.35	93.76 ± 0.70	0.75
River water1	5	5.01 ± 0.031	100.20 ± 0.62	0.62
	10	10.79 ± 0.018	107.90 ± 0.18	0.17
	50	50.04 ± 0.23	100.08 ± 0.46	0.46
River water 2	5	5.69 ± 0.015	113.80 ± 0.30	0.26
	10	10.69 ± 0.044	106.90 ± 0.44	0.41
	50	47.82 ± 0.077	95.64 ± 0.15	0.16
Human serum	5	5.01 ± 0.004	100.20 ± 0.08	0.08
	10	10.19 ± 0.063	101.90 ± 0.63	0.62
	50	47.77 ± 0.377	95.54 ± 0.75	0.79

RSD relative standard deviation

Fig. 6 **a** Overlap between the absorption band of Fe^{3+} and the excitation or emission band of the carbon dots (CDs). **b** Fluorescence decay curves of CDs in the presence and absence of Fe^{3+}. FL fluorescence

This phenomenon can be explained by there being a rapid reaction between the groups on the surface of the CDs and Fe^{3+}, while after introducing 1 mM of AA, Fe^{3+} and AA reacted with each other and the fluorescence intensity increased gradually.. The rising trend continued for 4–12 min, and then the fluorescence
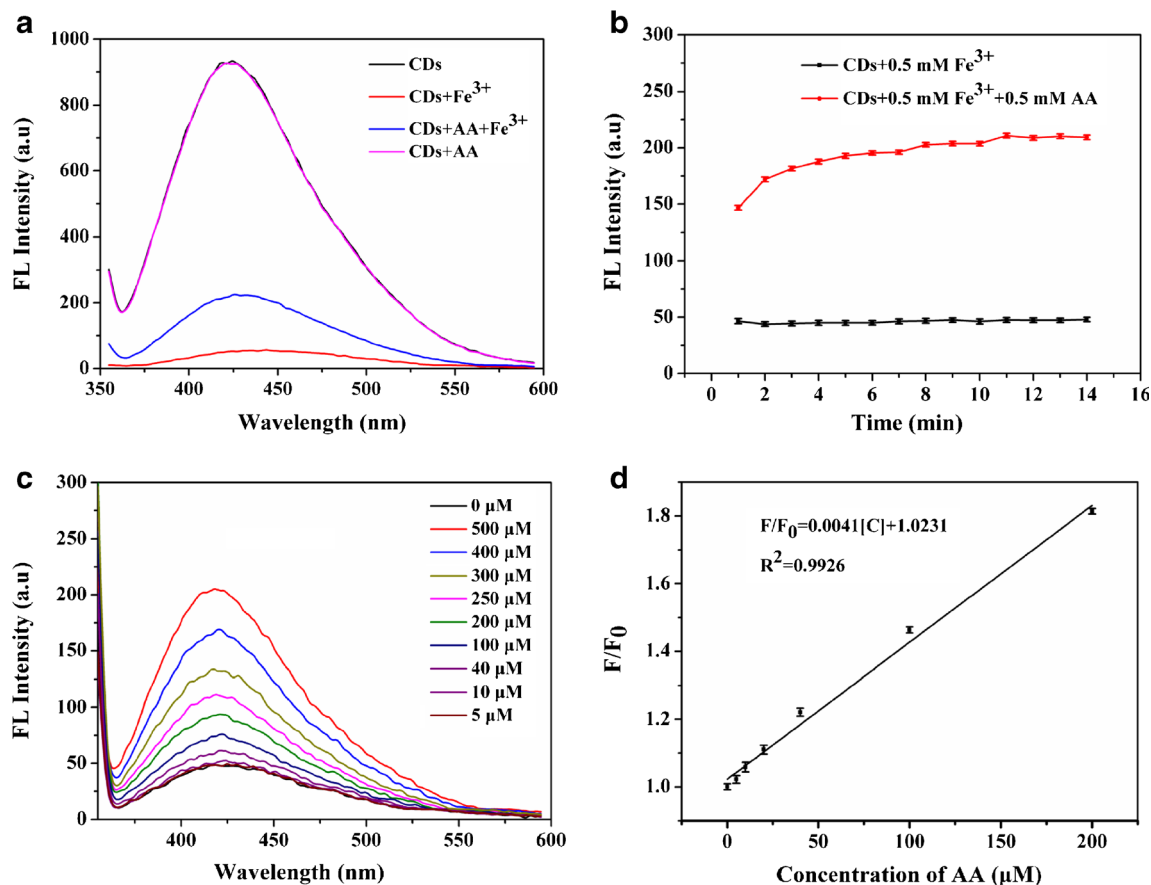

Fig. 7 **a** Fluorescence spectra of carbon dots (CDs), CDs and Fe^{3+}, CDs, Fe^{3+}, and ascorbic acid (AA), and CDs and AA. **b** The fluorescence intensity at different response times. **c** Fluorescence spectra of CDs in the presence of Fe^{3+} on addition of AA at different concentrations (0–500 μM). **d** F/F_0 versus AA concentration, where F_0 and F are the fluorescence areas of the CD–Fe^{3+} system in the absence and presence of AA. FL fluorescence

intensity became stable after 12 min. Therefore, the optimum recovery time was selected as 12 min.

The detection ability toward AA was studied by our adding different concentrations of AA (0–500 μM) to the CD–Fe^{3+} system (containing 0.5 mM Fe^{3+}) under the optimized reaction conditions. As shown in Fig. 7c, as the AA concentration increased, the fluorescence intensity gradually recovered.

Figure 7d shows that there was a good linear relationship between F/F_0 and the concentration of AA (range from 0 to 200 μM), with a correlation coefficient of 0.9926. The linear equation was $F/F_0 = 0.0041C + 1.0231$, where C is the concentration of AA. The LOD of AA was 5 μM ($3\sigma/K$). These results indicate that the CD–Fe^{3+} system can be used as a fluorescent off–on sensor for the detection of AA.
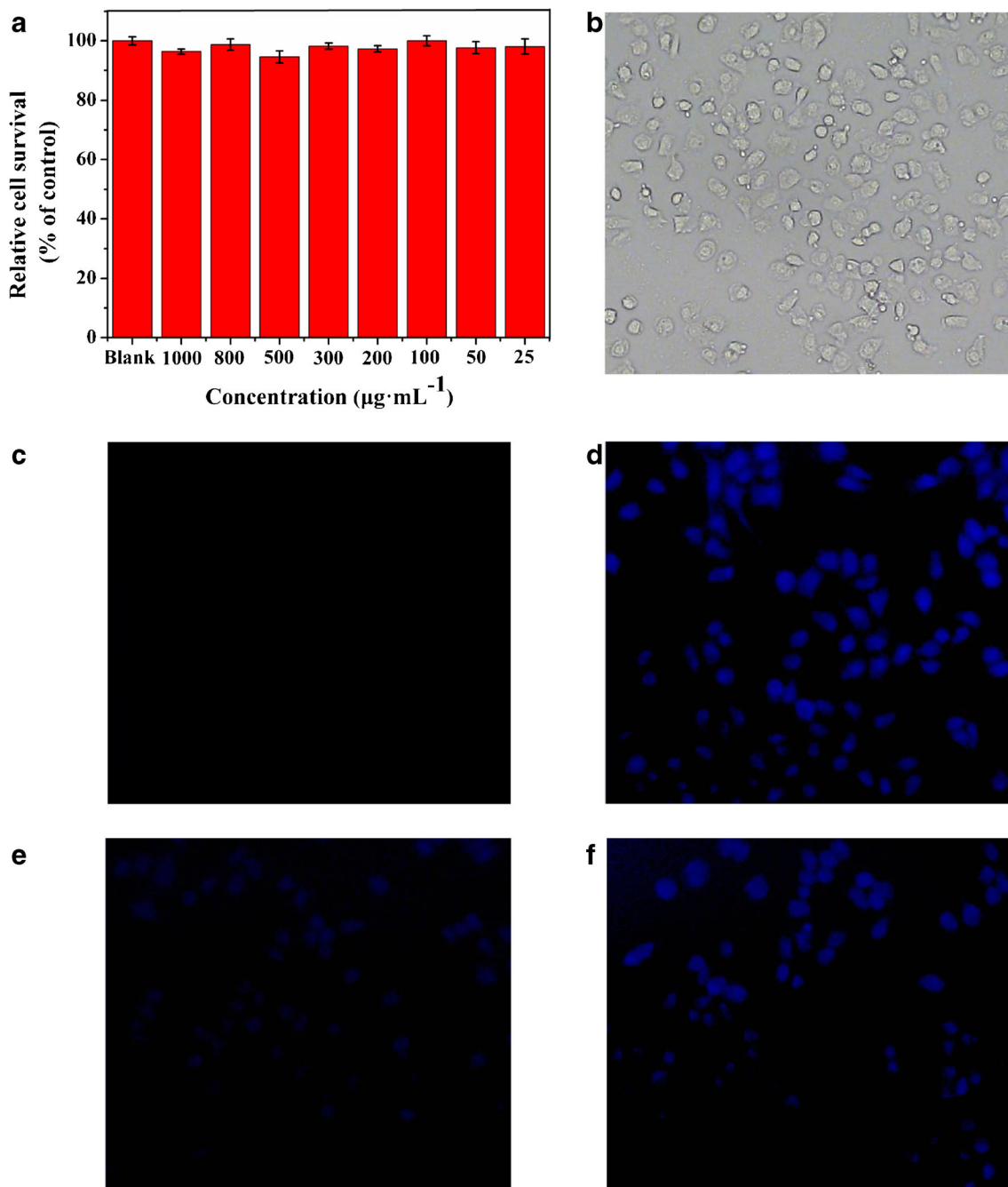
Fig. 8 **a** Effects of carbon dots (CDs) on the proliferation of A549 cells. **b** Images of A549 cells in bright field. **c** Fluorescence image of blank control (not incubated with CDs). **d** Fluorescence image of cells after incubation with CDs. **e** Fluorescence image of cells in the presence of CDs and Fe^{3+}. **f** Fluorescence image after further incubation with ascorbic acid

Cell cytotoxicity assay and cell imaging

To explore the toxicity and biocompatibility of CDs, and further try to apply the CDs for cell imaging, the cytotoxicity of CDs in A549 cells was studied by MTT measurements [54]. As depicted in Fig. 8a, the CDs had no obvious cell cytotoxic effect on cells in the concentration range from 25 to 1000 μg mL^{-1}. Because the CDs showed low toxicity toward the cells, they can be used for cell imaging and biomedical applications. Figure 8b–d shows that before addition of the CDs, the cells did not fluoresce, whereas after 3 h of incubation with the CDs, the cytoplasm of the cells showed bright blue fluorescence. This change can be ascribed to the CDs easily passing through the cell membrane and entering the cytoplasm. However, as shown in Fig. 8e, the blue fluorescence of cells became very weak after incubation with 0.4 mM Fe^{3+} for 30 min. The fluorescence was partially recovered after treatment with 0.4 mM AA for 30 min (Fig. 8f). Hence, the CDs can be used as a fluorescent on–off sensor for the qualitative analysis of Fe^{3+}, and the CD–Fe^{3+} system can be applied as a fluorescent off–on sensor for the qualitative analysis of AA in biological systems.

Conclusions

In summary, a green hydrothermal method was used to prepare CDs with high-intensity blue fluorescence by use of flowers of *O. fragrans* as green precursors. The CDs had high stability and good water solubility and were an effective fluorescent sensor for the direct detection of Fe^{3+} with a LOD of 5 nM. The satisfactory results for the detection of Fe^{3+} in real water samples and a human serum sample proved the practicability of the sensor. Moreover, on the basis of the selectivity and sensitivity of the CDs for Fe^{3+}, the CD–Fe^{3+} system was further developed as a fluorescent off–on sensor for the detection of AA. The LOD of AA was 5 μM. In addition, the CDs can be used for the fluorescence imaging of A549 cells with low toxicity and good biocompatibility. Moreover, Fe^{3+} (AA) can also be qualitatively analyzed by monitoring of the changes in cell fluorescence. Therefore, the CDs have great potential for application in sensing, bioimaging, and even disease diagnosis in analytical and biological fields as an ecofriendly sensor. However, the QY of the CDs and the recovery effect on AA need to be further explored.

Compliance with ethical standards

References

1. Ankireddy SR, Kim J. Highly selective and sensitive detection of calcium (II) ions in human serum using novel fluorescent carbon dots. Sensors Actuators B Chem. 2018;255:3425–33.
2. Karthik S, Saha B, Ghosh SK, Pradeep Singh ND. Photoresponsive quinoline tethered fluorescent carbon dots for regulated anticancer drug delivery. Chem Commun. 2013;49:10471–3.
3. Zhu S, Meng Q, Wang L, Zhang J, Song Y, Jin H, et al. Highly photoluminescent carbon dots for multicolor patterning, sensors, and bioimaging. Angew Chem Int Ed. 2013;52:3953–7.
4. Li W, Zhang HR, Chen S, Liu YL, Zhuang JL, Lei BF. Synthesis of molecularly imprinted carbon dot grafted YVO4:Eu^{3+} for the ratiometric fluorescent determination of paranitrophenol. Biosens Bioelectron. 2016;86:706–13.
5. Yang YX, Huo DQ, Wu HX, Wang XF, Yang JS, Bian MH, et al. N, P-doped carbon quantum dots as a fluorescent sensing platform for carbendazim detection based on fluorescence resonance energy transfer. Sensors Actuators B Chem. 2018;274:296–303.
6. Li HX, Yan X, Qiao SP, Lu GY, Su XG. Yellow-emissive carbon dot-based optical sensing platforms: cell imaging and analytical applications for biocatalytic reactions. ACS Appl Mater Interfaces. 2018;10:7737–44.
7. Gong PW, Sun L, Wang F, Liu XC, Yan ZQ, Wang MZ, et al. Highly fluorescent N-doped carbon dots with two-photon emission for ultrasensitive detection of tumor marker and visual monitor anticancer drug loading and delivery. Chem Eng J. 2019;356: 994–1002.
8. Liu YS, Li W, Wu P, Liu SX. Preparation and applications of carbon quantum dots prepared via hydrothermal carbonization method. Prog Chem. 2018;30:349–64.
9. Du FF, Li G, Gong XJ, Guo ZH, Shuang SM, Xian M, et al. Facile, rapid synthesis of N,P-dual-doped carbon dots as a label-free multifunctional nanosensor for Mn(VII) detection, temperature sensing and cellular imaging. Sensors Actuators B Chem. 2018;277:492–501.
10. Xu JC, Miao YQ, Zheng JX, Wang H, Yang YZ, Liu XG. Carbon dot-based white and yellow electroluminescent light emitting diodes with a record-breaking brightness. Nanoscale. 2018;10: 11211–21.
11. Bano D, Kumar V, Singh VK, Hasan SH. Green synthesis of fluorescent carbon quantum dots for the detection of mercury(II) and glutathione. New J Chem. 2018;42:5814–21.
12. Miao X, Qu D, Yang DX, Nie B, Zhao YK, Fan HY, et al. Synthesis of carbon dots with multiple color emission by controlled graphitization and surface functionalization. Adv Mater. 2018;30:1–8.

13. Zhou N, Zhang XW, Shi YP, Li ZL, Feng ZB. Nitrogen-doped carbon dot mediated fluorescence on-off assay for highly sensitive detection of I$^-$ and Br$^-$ ions. New J Chem. 2018;42:14332–9.

14. Bai ZJ, Yan FY, Xu JX, Zhang J, Wei JF, Luo YM, et al. Dual-channel fluorescence detection of mercuric (II) and glutathione by down- and up-conversion fluorescence carbon dots. Spectrochim Acta A. 2018;205:29–39.

15. Liu YA, Zhang TX, Wang R, Cui HN, Song HW. A facile and universal strategy for preparation of long wavelength emission carbon dots. Dalton Trans. 2017;46:16905–10.

16. Chen LY, Zhang YY, Duan BH, Gu ZZ, Guo YT, Wang HF, et al. Carbon dots prepared in different solvents with controllable structures: optical properties, cellular imaging and photocatalysis. New J Chem. 2018;42:1690–7.

17. Wang L, Zhou HS. Green synthesis of luminescent nitrogen-doped carbon dots from milk and its imaging application. Anal Chem. 2014;86:8902–5.

18. Vandarkuzhali SAA, Jeyalakshmi V, Sivaraman G, Singaravadivel S, Krishnamurthy KR, Viswanathan B. Highly fluorescent carbon dots from pseudo-stem of banana plant: applications as nanosensor and bio-imaging agents. Sensors Actuators B Chem. 2017;252: 894–900.

19. Bandi R, Gangapuram BR, Dadigala R, Eslavath R, Singh SS, Guttena V. Facile and green synthesis of fluorescent carbon dots from onion waste and their potential applications as sensor and multicolour imaging agents. RSC Adv. 2016;6:28633–9.

20. Bandi R, Dadigala R, Gangapuram BR, Guttena V. Green synthesis of highly fluorescent nitrogen-doped carbon dots from Lantana camara berries for effective detection of lead(II) and bioimaging. J Photochem Photobiol B. 2018;178:330–8.

21. Bhatt S, Bhatt M, Kumar A, Vyas G, Gajaria T, Paul P. Green route for synthesis of multifunctional fluorescent carbon dots from Tulsi leaves and its application as Cr(VI) sensors, bio-imaging and patterning agents. Colloids Surf B: Biointerfaces. 2018;167:126–33.

22. Xu J, Jie X, Xie FF, Yang HM, Wei WL, Xia ZN. Flavonoid moiety-incorporated carbon dots for ultrasensitive and highly selective fluorescence detection and removal of Pb^{2+}. Nano Res. 2018;11:3648–57.

23. Kumar A, Chowdhuri AR, Laha D, Mahto TK, Karmakar P, Sahu SK. Green synthesis of carbon dots from Ocimum sanctum for effective fluorescent sensing of Pb^{2+} ions and live cell imaging. Sensors Actuators B Chem. 2017;242:679–86.

24. Li LS, Jiao XY, Zhang Y, Cheng C, Huang K, Xu L. Green synthesis of fluorescent carbon dots from Hongcaitai for selective detection of hypochlorite and mercuric ions and cell imaging. Sensors Actuators B Chem. 2018;263:426–35.

25. Wang L, Tan NN, Hu JY, Wang H, Duan DZ, Ma L, et al. Analysis of the main active ingredients and bioactivities of essential oil from Osmanthus fragrans var. thunbergii using a complex network approach. BMC Syst Biol. 2017;11:144.

26. Wang LM, Li MT, Jin WW, Li S, Zhang SQ, Yu LJ. Variations in the components of Osmanthus fragrans Lour. essential oil at different stages of flowering. Food Chem. 2009;114:233–6.

27. Li HL, Chai Z, Shen GX, Li CY. Polyphenol profiles and antioxidant properties of ethanol extracts from Osmanthus fragrans (Thunb.) Lour. flowers. Pol J Food Nutr Sci. 2017;67:317–25.

28. Jiang YR, Mao SQ, Huang WS, Lu BY, Cai ZX, Zhou F, et al. Phenylethanoid glycoside profiles and antioxidant activities of Osmanthus fragrans Lour. flowers by UPLC/PDA/MS and simulated digestion model. J Agric Food Chem. 2016;64:2459–66.

29. Ilboudo O, Tapsoba I, Bonzi-Coulibaly YL, Gerbaux P. Targeting structural motifs of flavonoid diglycosides using collision-induced dissociation experiments on flavonoid/Pb^{2+} complexes. Eur J Mass Spectrom. 2012;18:465–73.

30. Perez CA, Wei YB, Guo ML. Iron-binding and anti-Fenton properties of baicalein and baicalin. J Inorg Biochem. 2009;103:326–32.

31. Murugan N, Sundramoorthy AK. Green synthesis of fluorescent carbon dots from Borassus flabellifer flowers for label-free highly selective and sensitive detection of Fe^{3+} ions. New J Chem. 2018;42:13297–307.

32. Zhou JL, Fang XY, Wang JQ, Zhao LG, Li Y, Tang F, et al. Structures and bioactivities of seven flavonoids from Osmanthus fragrans 'Jinqiu' essential oil extraction residues. Nat Prod Res. 2018;32:588–91.

33. Diao H, Li T, Zhang R, Kang Y, Liu W, Cui Y, et al. Facile and green synthesis of fluorescent carbon dots with tunable emission for sensors and cells imaging. Spectrochim Acta A. 2018;200:226–34.

34. Amjadi M, Hallaj T, Mayan MA. Green synthesis of nitrogen-doped carbon dots from lentil and its application for colorimetric determination of thioridazine hydrochloride. RSC Adv. 2016;6: 104467–73.

35. Xu Q, Su RG, Zhong J, Zhang LP, Guo YJ, Street J, et al. Synthesis of highly fluorescent yellow-green N-doped carbon nanorings for pH variation detection and bioimaging. Part Part Syst Charact. 2018;35:1800276.

36. Gao ZH, Lin ZZ, Chen XM, Zhong HP, Huang Z-y. A fluorescent probe based on N-doped carbon dots for highly sensitive detection of Hg^{2+} in aqueous solutions. Anal Methods. 2016;8:2297–304.

37. Li H, He H, Huang J, Wang CZ, Gu X, Gao Y, et al. A novel molecularly imprinted method with computational simulation for the affinity isolation and knockout of baicalein from Scutellaria baicalensis. Biomed Chromatogr. 2016;30:117–25.

38. Jiang K, Sun S, Zhang L, Wang Y, Cai C, Lin H. Bright-yellow-emissive N-doped carbon dots: preparation, cellular imaging, and bifunctional sensing. ACS Appl Mater Interfaces. 2015;7:23231–8.

39. Liu W, Diao H, Chang H, Wang H, Li T, Wei W. Green synthesis of carbon dots from rose-heart radish and application for Fe^{3+} detection and cell imaging. Sensors Actuators B Chem. 2017;241:190–8.

40. Bandi R, Devulapalli NP, Dadigala R, Gangapuram BR, Guttena V. Facile conversion of toxic cigarette butts to N,S-codoped carbon dots and their application in fluorescent film, security ink, bioimaging, sensing and logic gate operation. ACS Omega. 2018;3:13454–66.

41. Shi QQ, Li YH, Xu Y, Wang Y, Yin XB, He XW, et al. High-yield and high-solubility nitrogen-doped carbon dots: formation, fluorescence mechanism and imaging application. RSC Adv. 2014;4: 1563–6.

42. Liang Q, Wang YL, Lin FC, Jiang MS, Li PF, Huang B. A facile microwave-hydrothermal synthesis of fluorescent carbon quantum dots from bamboo tar and their application. Anal Methods. 2017;9: 3675–81.

43. Zhang J, Yang L, Yuan Y, Jiang J, Yu S-H. One-pot gram-scale synthesis of nitrogen and sulfur embedded organic dots with distinctive fluorescence behaviors in free and aggregated states. Chem Mater. 2016;28:4367–74.

44. Galande C, Mohite AD, Naumov AV, Gao W, Ci L, Ajayan A, et al. Quasi-molecular fluorescence from graphene oxide. Sci Rep. 2011;1:85.

45. Vezza T, Rodriguez-Nogales A, Algieri F, Utrilla MP, Rodriguez-Cabezas ME, Galvez J. Flavonoids in inflammatory bowel disease: a review. Nutrients. 2016;8:1–22.

46. Zhang S, Li J, Zeng M, Xu J, Wang X, Hu W. Polymer nanodots of graphitic carbon nitride as effective fluorescent probes for the detection of Fe^{3+} and Cu^{2+} ions. Nanoscale. 2014;6:4157–62.

47. Li S, Li Y, Cao J, Zhu J, Fan L, Li X. Sulfur-doped graphene quantum dots as a novel fluorescent probe for highly selective and sensitive detection of Fe^{3+}. Anal Chem. 2014;86:10201–7.

48. Guo XR, Yue GQ, Huang JZ, Liu C, Zeng Q, Wang LS. Label-free simultaneous analysis of Fe(III) and ascorbic acid using fluorescence switching of ultrathin graphitic carbon nitride nanosheets. ACS Appl Mater Interfaces. 2018;10:26118–27.

49. Akhgari F, Samadi N, Farhadi K. Fluorescent carbon dot as nanosensor for sensitive and selective detection of cefixime based on inner filter effect. J Fluoresc. 2017;27:921–7.

50. Li YH, Cai JB, Liu FJ, Yu HW, Lin F, Yang H, et al. Highly crystalline graphitic carbon nitride quantum dots as a fluorescent probe for detection of Fe(III) via an inner filter effect. Microchim Acta. 2018;185:1–7.

51. Chatzimarkou A, Chatzimitakos TG, Kasouni A, Sygellou L, Avgeropoulos A, Stalikas CD. Selective FRET-based sensing of 4-nitrophenol and cell imaging capitalizing on the fluorescent properties of carbon nanodots from apple seeds. Sensors Actuators B Chem. 2018;258:1152–60.

52. Luo X, Zhang W, Han Y, Chen X, Zhu L, Tang W, et al. N,S co-doped carbon dots based fluorescent "on-off-on" sensor for determination of ascorbic acid in common fruits. Food Chem. 2018;258:214–21.

53. Liu J, Wang L, Bao H. A novel fluorescent probe for ascorbic acid based on seed-mediated growth of silver nanoparticles quenching of carbon dots fluorescence. Anal Bioanal Chem. 2019;411:877–83.

54. Khan WU, Wang D, Zhang W, Tang Z, Ma X, Ding X, et al. High quantum yield green-emitting carbon dots for Fe(III) detection, biocompatible fluorescent ink and cellular imaging. Sci Rep. 2017;7:14866.